Structural, Magnetic, and Photomagnetic Studies of a Mononuclear Iron(II) Derivative Exhibiting an Exceptionally Abrupt Spin Transition. Light-Induced Thermal Hysteresis Phenomenon

Jean-François Létard,*,† Philippe Guionneau,†,‡ Louis Rabardel,† Judith A. K. Howard,‡ Andres E. Goeta,‡ Daniel Chasseau,† and Olivier Kahn*,†

Laboratoire des Sciences Moléculaires, Institut de Chimie de la Matière Condensée de Bordeaux, UPR CNRS No. 9048, 33608 Pessac, France, and Durham Chemical Crystallography Group, Chemistry Department, Durham University, South Road, Durham DH1 3LE, U.K.

Received January 29, 1998

The new spin-crossover compound $Fe(PM\text{-}BiA)_2(NCS)_2$ with PM-BiA = *N*-(2-pyridylmethylene)aminobiphenyl has been synthesized. The temperature dependence of $\chi_M T$ (χ_M = molar magnetic susceptibility and T = temperature) has revealed an exceptionally abrupt transition between low-spin (LS) ($S = 0$) and high-spin (HS) ($S = 2$) states with a well-reproducible hysteresis loop of 5 K ($T_{1/2}\downarrow = 168$ K and $T_{1/2}\uparrow = 173$ K). The crystal structure has been determined both at 298 K in the HS state and at 140 K in the LS state. The spin transition takes place without change of crystallographic space group (*Pccn* with $Z = 4$). The determination of the intermolecular contacts in the LS and HS forms has revealed a two-dimensional structural character. The enthalpy and entropy variations, ΔH and ΔS, associated with the spin transition have been deduced from heat capacity measurements. ΔS (= 58 J K^{-1} mol^{-1}) is larger than for other spin transition bis(thiocyanato) iron(II) derivatives. At 10 K the well-known LIESST (light-induced excited spin state trapping) effect has been observed within the SQUID cavity, by irradiating a single crystal or a powder sample with a Kr^+ laser coupled to an optical fiber. The magnetic behavior recorded under light irradiation in the warming and cooling modes has revealed a light-induced thermal hysteresis (LITH) effect with $35 < T_{1/2} < 77$ K. The HS → LS relaxation after LIESST has been found to deviate from first-order kinetics. The kinetics has been investigated between 10 and 78 K. A thermally activated relaxation behavior at elevated temperatures and a nearly temperature independent tunneling mechanism at low temperatures have been observed. The slow rate of tunneling from the metastable HS state toward the ground LS state may be explained by the unusually large change in Fe−N bond lengths between these two states.

Introduction

In some transition metal compounds, in particular in those containing $3d^4$ −$3d^7$ metal ions in octahedral surroundings, a spin crossover may occur between a low-spin (LS) and a high-spin (HS) state. For iron(II) derivatives the LS state is $S = 0$ and the HS state $S = 2$, and the crossover may be induced by a change of temperature or of pressure or by light irradiation.[1] Spin conversions have been observed in the solid state as well as in solution. In the latter case the process is essentially molecular, and the spin conversion is very gradual, obeying a Boltzmann distribution law between two spin states.[2] When the process takes place in the solid state, it may be cooperative if the intersite interactions are strong enough. This cooperativity may lead to very abrupt transitions along with thermal hysteresis. The thermal hysteresis width defines the temperature range of bistability for the system.[3]

One of our main goals in the field of spin-crossover compounds is to design systems exhibiting a strong cooperativity. We are presently exploring two strategies to reach this goal. The former is based on the polymeric approach. It has been suggested and experimentally confirmed that the cooperativity can be magnified by designing polymeric structures in which the active sites are linked to each other by chemical bridges. Some compounds of this kind have been found to display thermal hysteresis widths reaching ca. 40 K.[4] These polymeric compounds, however, are not strictly molecular anymore. The latter strategy is based on the supramolecular approach. The objective is then to design strongly cooperative spin-crossover assemblies consisting of mononuclear molecules,

† Institut de Chimie de la Matière Condensée de Bordeaux.
‡ Durham Chemical Crystallography Group.

(1) (a) Goodwin, H. A. *Coord. Chem. Rev.* **1976**, *18*, 293. (b) Gütlich, P. *Struct. Bonding (Berlin)* **1981**, *44*, 83. (c) König, E. *Prog. Inorg. Chem.* **1987**, *35*, 527. (d) Gütlich, P.; Hauser, A. *Coord. Chem. Rev.* **1990**, *97*, 1. (e) König, E. *Struct. Bonding (Berlin)* **1991**, *76*, 51. (f) Gütlich, P.; Hauser, A.; Spiering, H. *Angew. Chem., Int. Ed. Engl.* **1994**, *33*, 2024 and references therein. (g) Gütlich, P.; Jung, J.; Goodwin, H. In *Molecular Magnetism: From Molecular Assemblies to the Devices*; Coronado et al., Eds.; Kluwer: Dordrecht, The Netherlands, 1996; p 327.
(2) Beattie, J. K. *Adv. Inorg. Chem.* **1988**, *32*, 2.
(3) (a) Kahn, O.; Launay, J. P. *Chemtronics* **1988**, *3*, 140. (b) Zarembowitch, J.; Kahn, O. *New J. Chem.* **1991**, *15*, 181. (c) Kahn, O. *Molecular Magnetism*; VCH: New York, 1993.
(4) (a) Vreugdenhil, W.; van Diemen, J. H.; de Graaff, R. A. G.; Haasnoot, J. G.; Reedgijk, J.; van der Kraan, A. M.; Kahn, O.; Zarembowitch, *J. Polyhedron* **1990**, *9*, 2971. (b) Kahn, O.; Kröber, J.; Jay, C. *Adv. Mater.* **1992**, *4*, 718. (c) Kröber, J.; Audière, J. P.; Claude, R.; Codjovi, E.; Kahn, O., Haasnoot, J. G.; Grolière, F.; Jay C.; Bousseksou, A.; Linarès, J.; Varret, F.; Gonthier-Vassal, A. *Chem. Mater.* **1994**, *6*, 1404. (d) Lavrenova, L G.; Ikorskii, V. N.; Varnek, V. A.; Oglezneva, I. M.; Larionov, S. V. *Polyhedron* **1995**, *14*, 1333. (e) Kahn, O.; Codjovi, E.; Garcia, Y.; van Koningsbruggen P. J.; Lapouyade, R.; Sommier, L. In *Molecule-Based Magnetic Materials*; Turnbull, M. M., Sugimoto, T., Thompson, L. K., Eds.; ACS Symposium Series 644; American Chemical Society, Washington, DC, 1996.

S0020-1669(98)00107-4 CCC: $15.00
Published on Web 08/07/1998

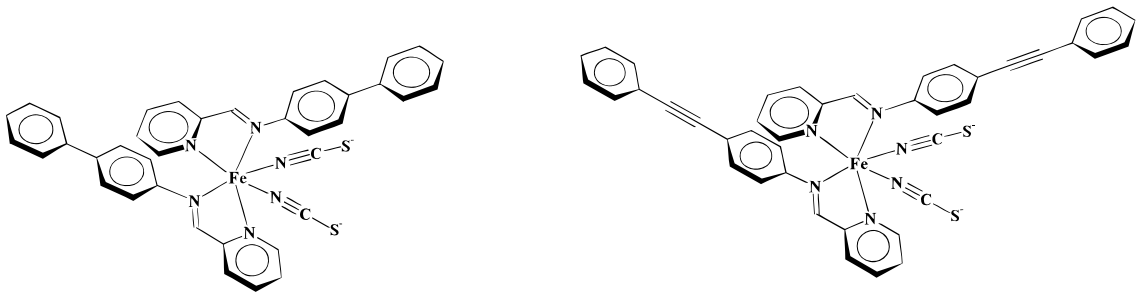

$Fe(PM\text{-}BiA)_2(NCS)_2$ **$Fe(PM\text{-}PEA)_2(NCS)_2$**

Figure 1. Schematic representation of *cis*-bis(thiocyanato)bis(*N*-(2-pyridylmethylene)aminobiphenyl)iron(II), $Fe(PM\text{-}BiA)_2(NCS)_2$, and *cis*-bis(thiocyanato)bis(*N*-(2′-pyridylmethylene)-4-(phenylethynyl)anilino)iron(II), $Fe(PM\text{-}PEA)_2(NCS)_2$.

with through-space rather than through-bond interactions. Our first question was, Could such molecular lattices could also exhibit wide thermal hysteresis loops? To the best of our knowledge, the hysteresis widths obtained so far with mononuclear spin-crossover iron(II) derivatives do not exceed ≈10 K, except for systems in which the spin transition was influenced by uncoordinated solvent molecules, intraligand substitution, or ligand replacement.

Our starting idea was to achieve strong intermolecular interactions through the stacking of aromatic rings. Along this line we have already reported on two findings: (i) We reported the first mononuclear spin-crossover derivative, *cis*-bis(thiocyanato)-bis[*N*-(2′-pyridylmethylene)-4-(phenylethynyl)aniline]iron(II), $Fe(PM\text{-}PEA)_2(NCS)_2$ (Figure 1), with a thermal hysteresis loop of 37 K.[5] The absence of solvent molecule in the lattice eliminates the possibility of apparent hysteresis, resulting from the synergy between LS → HS transformation and removal of noncoordinated solvent molecules,[6] as observed, for instance, for $[Fe(2\text{-pic})_3]Cl_2 \cdot H_2O$ (2-pic = 2-picolylamine).[7] The crystal structure of $Fe(PM\text{-}PEA)_2(NCS)_2$ solved both at room temperature (HS state) and at 140 K (LS state) suggests that the cooperativity may be attributed to both intermolecular π interactions between phenyl rings and interlocking of molecular units.[5] (ii) We reported the first example of a mononuclear iron(II) spin-crossover compound, *cis*-bis(thiocyanato)-bis[*N*-(2-pyridylmethylene)aminobiphenyl]iron(II), $Fe(PM\text{-}BiA)_2(NCS)_2$ (Figure 1), with large negative cubic hyperpolarizability at room temperature.[8] Negative third-order nonlinearities are uncommon and have the property to induce a self-defocusing effect, which can be applied to eliminate the nonlinear optical auto-optical annihilation of a potential all-optical device.[9]

In the present paper we study in more detail the $Fe(PM\text{-}BiA)_2(NCS)_2$ compound. The magnetic susceptibility, the thermogravimetry analysis, and the crystal structure at both temperatures 298 K (HS spin state) and 140 K (LS state) of $Fe(PM\text{-}BiA)_2(NCS)_2$ will be reported. The LIESST (light-induced excited spin state trapping) of $Fe(PM\text{-}BiA)_2(NCS)_2$ recorded at 10 K within a SQUID cavity through light irradiation will be presented. We will also present a new phenomenon: the magnetic behavior recorded with decreasing and increasing temperatures under light irradiation shows an unexpected thermal hysteresis. We propose to call this effect LITH for light-induced thermal hysteresis.

Experimental Section

Syntheses. The compound *cis*-bis(thiocyanato)bis(*N*-(2-pyridylmethylene)aminobiphenyl)iron(II), $Fe(PM\text{-}BiA)_2(NCS)_2$, was prepared as follows. The Schiff base PM-BiA was synthesized from 2-pyridinecarbaldehyde and aminobiphenyl. ^1H NMR ($CDCl_3$, 200 MHz): δ 7.30−7.49 (6H, m), 7.62−7.66 (4H, t), 7.83−7.84 (1H, t), 8.22−8.25 (1H, d), 8.68 (s, 1H), 8.71−8.75 (d, 1H). MS (*e*/*z*): 258 (M^+, 100), 231 (31), 152 (36), 79 (20). $Fe(PM\text{-}BiA)_2(NCS)_2$ was obtained in the form of two kinds of powder samples, noted **1** and **2**, as well as single crystals. The powder sample **1** was prepared under a nitrogen atmosphere as follows: In 20 mL of freshly distilled methanol were dissolved iron(II) sulfate heptahydrate, $Fe(SO_4)_2 \cdot 7H_2O$ (2.7 g, 9.7 mmol), and potassium thiocyanate, KNCS (1.8 g, 19 mmol), in the presence of some crystals of ascorbic acid to prevent Fe^{2+} oxidation. The colorless solution of $Fe(NCS)_2$ was separated from the white precipitate of potassium sulfate by filtration and added dropwise to a stoichiometric amount of *N*-(2-pyridylmethylene)aminobiphenyl (5 g, 19 mmol) in 20 mL of methanol. After 1 h a green precipitate of $Fe(PM\text{-}BiA)_2(NCS)_2$ (**1**) was formed. It was filtered off, washed several times with diethyl ether, and dried in a nitrogen stream. Anal. Calcd for $FeC_{38}H_{28}N_6S_2$: C, 66.28; H, 4.07; N, 12.21; S, 9.30; Fe, 8.14. Found: C, 63.76; H, 4.08; N, 11.82; S, 9.38; Fe, 7.81. For the powder sample **2**, the synthetic method only differed by use of an excess of ligand PM-BiA (1 g, 3.88 mmol) with respect to $Fe(SO_4)_2 \cdot 7H_2O$, (0.27 g, 0.97 mmol) and KNCS (0.189 g, 1.94 mmol). The addition of $Fe(NCS)_2$ instantaneously led to a green precipitate of **2**. Anal. Calcd for $FeC_{38}H_{28}N_6S_2$: C, 66.28; H, 4.07; N, 12.21; S, 9.30; Fe, 8.14. Found: C, 66.26; H, 4.09; N, 12.03; S, 8.90; Fe, 8.32. Single crystals were obtained by slow diffusion in methanol of *N*-(2-pyridylmethylene)-aminobiphenyl, PM-BiA, and $Fe(NCS)_2$, using an H double-tube glass. Anal. Calcd for $FeC_{38}H_{28}N_6S_2$: C, 66.28; H, 4.07; N, 12.21; S, 9.30; Fe, 8.14. Found: C, 66.16; H, 4.11; N, 12.25; S, 9.32; Fe, 7.55.

Crystallographic Data Collection and Structure Determination. The crystal structure at room temperature (298 K) was determined using a four-circle diffractometer (Cu Kα radiation) equipped with a point detector. This structure of the compound in the HS state was briefly described in a preliminary communication.[8] Cooling down the crystal without damage was possible only by decreasing the temperature quite slowly at a velocity of 0.5 K min^{-1}, and without exposing the crystal to X-ray radiation. A full set of intensities was collected at 140 K using a Siemens Smart-CCD diffractometer with graphite-monochromated Mo Kα radiation (0.7107 Å).[10] Cell parameters were refined using the centroid values of 292 reflections. Data collection was based

(5) Létard, J.-F.; Guionneau, P.; Codjovi, E.; Lavastre, O.; Bravic, G.; Chasseau, D.; Kahn, O. *J. Am. Chem. Soc.* **1997**, *119*, 10861.
(6) Garcia, Y.; van Koningsbruggen P. J.; Codjovi, E.; Lapouyade, R.; Kahn, O.; Rabardel, L. *J. Mater. Chem.* **1997**, *7*, 857.
(7) (a) Sorai, M.; Ensling, J.; Hasselbach, K. M.; Gütlich, P. *Chem. Phys.* **1977**, *20*, 197. (b) Gütlich, P.; Köppen, H.; Steinhäuser, H. G. *Chem. Phys. Lett.* **1980**, *74*, 3.
(8) Létard, J.-F.; Montant, S.; Guionneau, P.; Martin, P.; Le Calvez, A.; Freysz, E.; Chasseau, D.; Lapouyade, R.; Kahn, O. *J. Chem. Soc., Chem. Commun*. **1997**, 745.
(9) Dirk, C. W.; Herndon, W. C.; Cervantes-Lee, F.; Selnau, H.; Martinez, S.; Kalamegham, P.; Tan, A.; Campos, G.; Velez, M.; Zyss, J.; Ledoux, I.; Cheng, L.-T. *J. Am. Chem. Soc.* **1995**, *117*, 2214.
(10) *SMART Version 4.050*; Siemens Analytical X-ray Instruments: Madison, WI, 1995.

Table 1. Selected Crystal Data for $Fe(PM\text{-}BiA)_2(NCS)_2$ at 298 and 140 K

	$T = 298$ K[a]	$T = 140$ K
formula	$FeC_{38}H_{28}N_6S_2$	
fw	688.7	
space group	*Pccn*	*Pccn*
a, Å	12.949(7)	12.370(3)
b, Å	15.183(2)	14.764(3)
c, Å	17.609(5)	18.281(4)
V, Å^3	3462(2)[b]	3338[b]
D(calcd), g cm^{-3}	1.33	1.37
Z	4	4
μ, cm^{-1}	49.21	6.14
unit cell	25 reflns	292 reflns
scan type	$\omega-\theta$	ω
no. of indep reflns	3331	3831
refinement on	*F*	F^2
R(*F*)	0.045	0.043
	$\omega R(F)$ 0.035	$\omega R(F^2)$ 0.087
S	1.30	1.06
max peak in final ($\Delta\rho$), e Å^{-3}	0.20/−0.15	0.35/−0.45

[a] From ref 8. [b] The volume of the unit cell at 160 K; i.e., just above the transition was found as 3387 Å^3.

on ω-scans in such a way that an initial 180° scan range consisting of 0.3° intervals was followed by three further 130°, 180°, and 130° scans with Ψ offset of 88°, 180°, and 268°, respectively. Such a hemisphere corresponds to a reciprocal space of $2\theta_{max} = 55.13°$. The frame data were integrated using the SAINT program,[11] and the data were corrected for absorption using SADABS.[12] Transmission factors were in the range 0.629−0.828. The 34 006 collected reflections were reduced to 3831 unique reflections ($R_{int} = 3.79\%$), of which 2587 were observed. The structure was solved and refined using the Siemens Shelxtl plus package.[13] The standard deviations of atomic parameters obtained at 140 K are weaker than those obtained at 298 K, owing to a larger number of observed reflections. Selected crystal data are given in Table 1. The volume of the unit cell (*V*) was measured every 20 K as the temperature (*T*) was lowered from room temperature down to 140 K. The $V = f(T)$ curve is nearly linear down to 160 K, and the slope is about 0.5 Å^3 K^{-1}. From 160 K down to 140 K, the volume decrease is much faster, with a slope of 2.5 Å^3 K^{-1}.

X-ray Powder Patterns. These were carried out at room temperature, using a D500 Siemens powder diffractometer (Cu Kα, λ = 1.540 18 Å) with $2-\Theta$ scans from 4° to 32°.

Physical Measurements. Elemental analyses were performed by the Service Central d'Analyse (CNRS) in Vernaison, France. Thermogravimetric measurements were carried out with a Setaram apparatus in the temperature range 300−600 K under ambient atmosphere. The heat capacities were measured with a Perkin-Elmer DSC-7 calorimeter whose cell was cooled at a velocity of 2 K min^{-1}. Magnetic susceptibility measurements were carried out over the temperature range 300−80 K, by using a Manics DSM-8 fully automatized Faraday-type magnetometer equipped with an DN-170 Oxford Instruments continuous-flow cryostat and a BE 15f Bruker electromagnet operating at ca. 0.8 T. Two samples were studied, one consisting of well-shaped single crystals, the other one of the powder, both weighing around 20 mg. Data were corrected for the magnetization of the sample holder and for diamagnetic contributions. LIESST experiments were carried out using a Kr^+ laser coupled through an optical fiber to the cavity of a MPMS-55 Quantum Design SQUID magnetometer. For all the wavelengths used (λ = 488.0−514.5 nm, 530.9 nm, 647.1−679.4 nm, and 752.5−799.3 nm) the output power was adjusted to 50 mW.

(11) *SAINT Version 4.050*; Siemens Analytical X-ray Instruments: Madison, WI, 1995.
(12) Sheldrick, G. M. SADABS Empirical Absorption Program; University of Göttingen: Göttingen, Germany.
(13) Sheldrick, G. M. *SHELXTL-Plus. Release 4.1*; Siemens Analytical X-ray Instruments Inc.: Madison, WI, 1991.

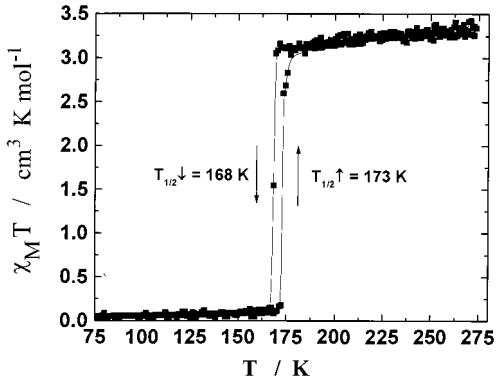

Figure 2. $\chi_M T$ versus *T* plots for single crystals of $Fe(PM\text{-}BiA)_2(NCS)_2$ in both cooling and warming modes. The temperature was varied at a rate of 1 K min^{-1} without overshooting. $T_{1/2}\downarrow$ and $T_{1/2}\uparrow$ are defined as the inversion temperatures for which there are 50% of LS and 50% of HS molecules in the cooling and warming modes, respectively.

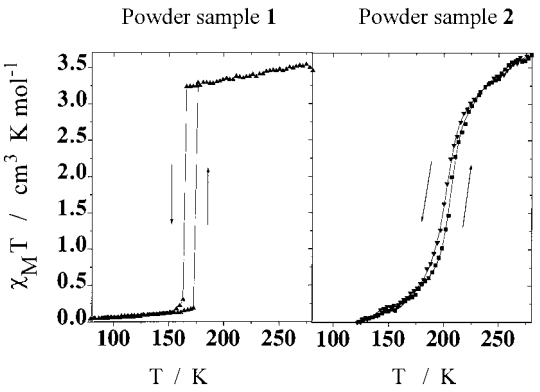

Figure 3. $\chi_M T$ versus *T* plots for the powder samples **1** and **2**. The temperature was varied at a rate of 3 K min^{-1}.

Results and Discussion

Magnetic Behavior. The magnetic properties of the samples were expressed in the form of the $\chi_M T$ versus *T* curves, where χ_M stands for the molar magnetic susceptibility and *T* the temperature. In a first approximation the HS molar fraction, γ_{HS}, may be deduced from $\chi_M T$ through

$$\gamma_{HS} = \chi_M T/(\chi_M T)_{HT} \quad (1)$$

where $(\chi_M T)_{HT}$ is the high-temperature limit of $\chi_M T$. Figure 2 shows the $\chi_M T$ versus *T* curve for a sample consisting of single crystals selected under the binocular lens. At room temperature $\chi_M T$ is equal to 3.5 cm^3 K mol^{-1}, which corresponds to what is expected for an Fe^{2+} ion in the HS state, decreases smoothly down to 3.06 cm^3 K mol^{-1} as *T* is lowered down to 169.2 K, and then drops very abruptly within 2 K ($T_{1/2}\downarrow$ = 168 K) down to 0.15 cm^3 K mol^{-1} at 167.2 K. At 80 K, $\chi_M T$ is close to 0. In the warming mode an abrupt variation of $\chi_M T$, occurring within 1 K, was observed at $T_{1/2}\uparrow$ = 173 K. More precisely $\chi_M T$ is equal to 0.17 cm^3 K mol^{-1} at 172.4 K, and to 2.60 cm^3 K mol^{-1} at 173.3 K. Successive thermal cycles did not modify the thermal hysteresis loop. It was also checked that the loop did not depend on the magnitude of the field up to 15 kOe.

The magnetic behavior of powder samples (Figure 3) strongly depends on the way the synthesis was performed (see Experimental Section). The powder sample **1** essentially behaves as the crystalline sample. On the other hand, the powder sample **2** exhibits a much more gradual spin transition with $T_{1/2}\downarrow$ = 205 K and $T_{1/2}\uparrow$ = 209 K, as already described in our preliminary communication.[8] Such a difference strongly suggests that the

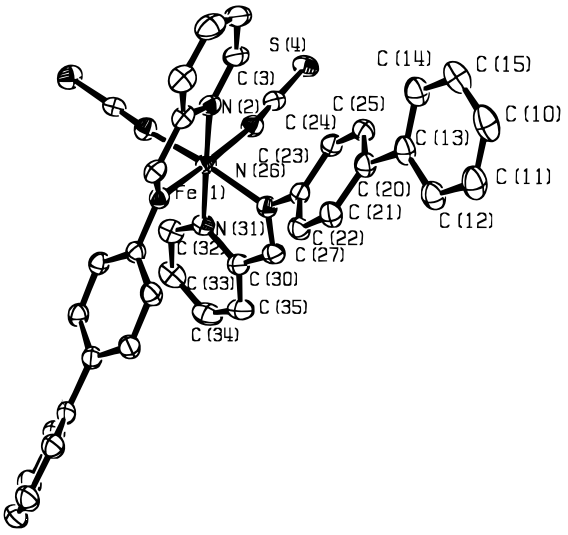

Figure 4. Perspective view of the $Fe(PM\text{-}BiA)_2(NCS)_2$ molecule at 140 K, including the non-hydrogen atom numbering. Hydrogen atoms are omitted for clarity.

Table 2. Bond Lengths (Å)[a]

	$T = 298$ K[b]	$T = 140$ K		$T = 298$ K[b]	$T = 140$ K
N(2)−Fe(1)	2.041(8)	1.939(2)	C(22)−C(23)	1.395(12)	1.395(4)
N(26)−Fe(1)	2.251(8)	1.966(2)	C(23)−C(24)	1.392(12)	1.389(4)
N(31)−Fe(1)	2.230(8)	1.964(2)	C(24)−C(25)	1.371(12)	1.385(4)
N(2)−C(3)	1.134(10)	1.162(3)	C(25)−C(20)	1.416(12)	1.396(4)
C(3)−S(4)	1.626(10)	1.636(3)	C(23)−N(26)	1.415(10)	1.438(3)
C(10)−C(11)	1.382(12)	1.376(4)	N(26)−C(27)	1.236(10)	1.294(3)
C(11)−C(12)	1.387(12)	1.389(4)	C(27)−C(30)	1.507(12)	1.454(4)
C(12)−C(13)	1.388(12)	1.390(4)	C(30)−N(31)	1.364(12)	1.359(3)
C(13)−C(14)	1.386(12)	1.397(4)	N(31)−C(32)	1.333(12)	1.345(3)
C(14)−C(15)	1.384(12)	1.393(4)	C(32)−C(33)	1.373(10)	1.377(4)
C(13)−C(20)	1.479(12)	1.486(4)	C(33)−C(34)	1.384(10)	1.382(4)
C(20)−C(21)	1.401(12)	1.394(4)	C(34)−C(35)	1.380(10)	1.379(4)
C(21)−C(22)	1.357(12)	1.385(4)	C(35)−C(30)	1.407(10)	1.382(4)

[a] The numbers in parentheses are estimated standard deviations in the least significant digits. [b] From ref 8.

use of an excess of ligand leads to a compound whose crystal structure is not the same as that of the single crystals. This was confirmed by the X-ray powder pattern (see below).

Description of the Structures. The crystal structure of $Fe(PM\text{-}BiA)_2(NCS)_2$ was determined by X-ray diffraction at both 298 and 140 K. The space group (*Pccn*) is retained in both states. Figure 4 shows a perspective view of the molecule together with the numbering of the atoms included in the asymmetric unit. Each iron atom is surrounded by six nitrogen atoms belonging to two NCS^- groups in cis positions and two PM-BiA ligands. Bond lengths and angles related to the HS (298 K) and LS (140 K) forms are compared in Tables 2−4. Figure 5 shows the structures at both 298 and 140 K. It can be noticed that the molecule is chiral and that each unit cell contains two right-handed and two left-handed enantiomers. The molecular packing can be described as sheets of molecules parallel to the *ac* plane. Figure 6 presents such a sheet at 298 and 140 K. The volume of the unit cell decreases of 3.65% between 298 and 140 K. On the other hand, while two of the cell parameters, *a* and *b*, decrease as well, the third one, *c*, increases significantly.

A. High-Spin Crystal Structure. The structure of $Fe(PM\text{-}BiA)_2(NCS)_2$ at 298 K has already been reported.[8] Briefly, it can be noticed that the NCS^- groups are linear (S(4)−C(3)−N(2) = 178.2(9)°), whereas the Fe−N−C(S) linkages are slightly bent (169.0(9)°). The Fe−N(CS^-) distances (Fe−N(2) = 2.041(8) Å) are shorter than the Fe−N(organic ligand) distances (Fe−N(26) = 2.251(8) Å and Fe−N(31)= 2.230(8) Å), which induces a pronounced distortion of the FeN_6

Table 3. Selected Bond Angles and Dihedral Angles (deg)[a]

	$T = 298$ K[b]	$T = 140$ K
N(2)−Fe(1)−N(31)	90.2(3)	90.8(7)
N(2)−Fe(1)−N(26)	96.0(3)	93.0(6)
N(26)−Fe(1)−N(31)	74.3(8)	80.7(9)
C(3)−N(2)−Fe(1)	169.0(9)	172.5(0)
S(4)−C(3)−N(2)	178.2(9)	178.4(1)
C(30)−N(31)−C(32)	120.1(9)	117.6(2)
N(31)−C(32)−C(33)	122.8(9)	122.4(7)
C(32)−C(33)−C(34)	118.4(10)	119.7(9)
C(33)−C(34)−C(35)	119.4(10)	118.3(9)
C(34)−C(35)−C(30)	120.0(10)	119.4(0)
C(35)−C(30)−N(31)	118.9(10)	122.3(1)
Fe(1)−N(31)−C(32)	125.8(7)	127.9(2)
Fe(1)−N(31)−C(30)	113.6(7)	114.4(5)
N(31)−C(30)−C(27)	116.3(7)	113.3(0)
C(30)−C(27)−N(26)	118.5(9)	115.3(8)
C(27)−N(26)−Fe(1)	116.4(7)	115.8(1)
C(23)−N(26)−Fe(1)	126.7(7)	125.6(2)
C(27)−N(26)−C(23)	115.6(9)	117.9(5)
N(26)−C(23)−C(24)	120.3(9)	119.7(0)
C(23)−C(24)−C(25)	118.0(10)	119.3(0)
C(24)−C(25)−C(20)	122.8(10)	121.7(2)
C(20)−C(21)−C(22)	122.0(10)	122.0(1)
C(21)−C(22)−C(23)	119.9(10)	119.5(8)
C(22)−C(23)−C(24)	120.8(10)	120.1(5)
C(25)−C(20)−C(21)	116.3(10)	117.8(4)
C(25)−C(20)−C(13)	122.2(10)	121.0(4)
C(20)−C(13)−C(12)	118.4(10)	120.2(5)
C(13)−C(12)−C(11)	118.6(10)	118.6(0)
C(12)−C(11)−C(10)	120.6(10)	120.4(3)
C(11)−C(10)−C(15)	121.2(10)	119.6(5)
C(10)−C(15)−C(14)	117.9(10)	120.3(7)
C(15)−C(14)−C(13)	121.4(10)	120.5(8)
C(23)−N(26)−Fe(1)−N(2)	86.3(10)	94.0(3)
N(26)−C(27)−C(30)−N(31)	−2.0(1)	−1.9(3)
C(12)−C(13)−C(20)−C(21)	41.8(10)	33.8(3)
C(22)−C(23)−N(26)−C(27)	−42.8(10)	−55.5(3)
C(23)−N(26)−C(27)−C(30)	175.7(10)	176.5(3)

[a] The numbers in parentheses are estimated standard deviations in the least significant digits. [b] From ref 8.

Table 4. Intermolecular Distances (Å) Shorter than van der Waals Contacts at 140 and 298 K and Corresponding Fe−Fe Distances[a]

	$T = 298$ K	$T = 140$ K
$C(14)-C(27)_{i'}$	3.599	3.456
$C(14)-C(35)_{i'}$	3.684	3.522
$C(14)-C(30)_{i'}$	3.464	3.500
$C(15)-N(2)_{i'}$	3.406	3.602
$C(15)-C(3)_{i'}$	3.348	3.416
$C(20)-C(35)_{i'}$	3.683	3.571
$C(27)-C(12)_{i'}$	3.599	3.456
$C(12)-C(12)_{i''''}$	3.657	3.337
$S(4)-C(22)_{i''}$	3.608	3.764
$S(4)-C(21)_{i''}$	3.416	3.437
$C(14)-C(33)_{i'''}$	3.457	3.409
$C(15)-C(33)_{i'''}$	3.426	3.489
$C(27)-S(4)_{i'''}$	3.776	3.818
$Fe(1)-Fe(1)_{i'}$	11.708	11.269
$Fe(1)-Fe(1)_{i''}$	10.331	10.176
$Fe(1)-Fe(1)_{i'''}$	8.805	9.141
$Fe(1)-Fe(1)_{i''''}$	12.949	12.370

[a] Highest standard deviations at 298 and 140 K are 0.010 and 0.003 Å (S−C), 0.012 and 0.005 Å (C−C), and 0.010 and 0.004 Å (C−N), respectively. Nomenclature for a molecule origin: i ($^3/_4$, $^1/_4$, *z*); i′ (1 − *x*, $^1/_2$ + *y*, $^1/_2$ − *z*); i″ (1 − *x*, 1 − *y*, − *z*); i‴ (*x*, $^1/_2$ − *y*, $^1/_2$ + *z*), and i⁗ (−1 + *x*, *y*, *z*). The interactions i−i′ and i−i⁗ correspond to intrasheet distances, and interactions i−i″ and i−i‴ to intersheet distances.

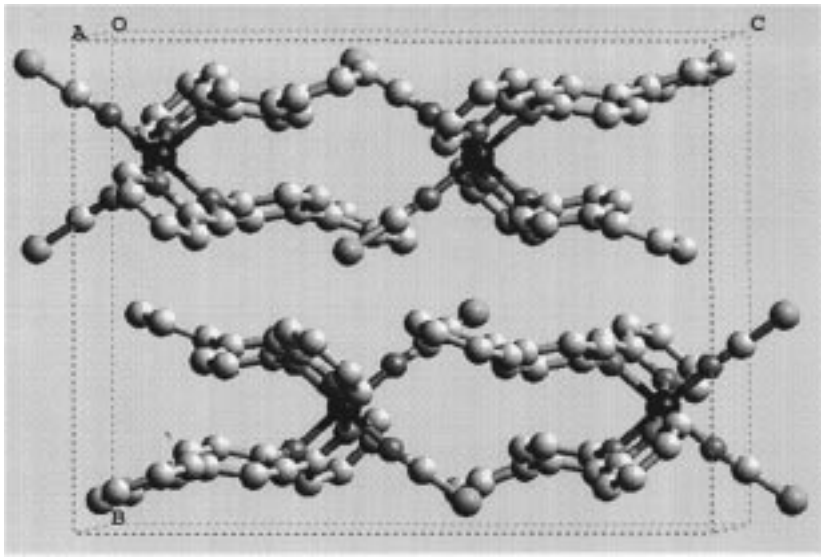

Figure 5. Structure of $Fe(PM\text{-}BiA)_2(NCS)_2$ at 140 K, projected along the *a* axis. Hydrogen atoms are omitted for clarity.

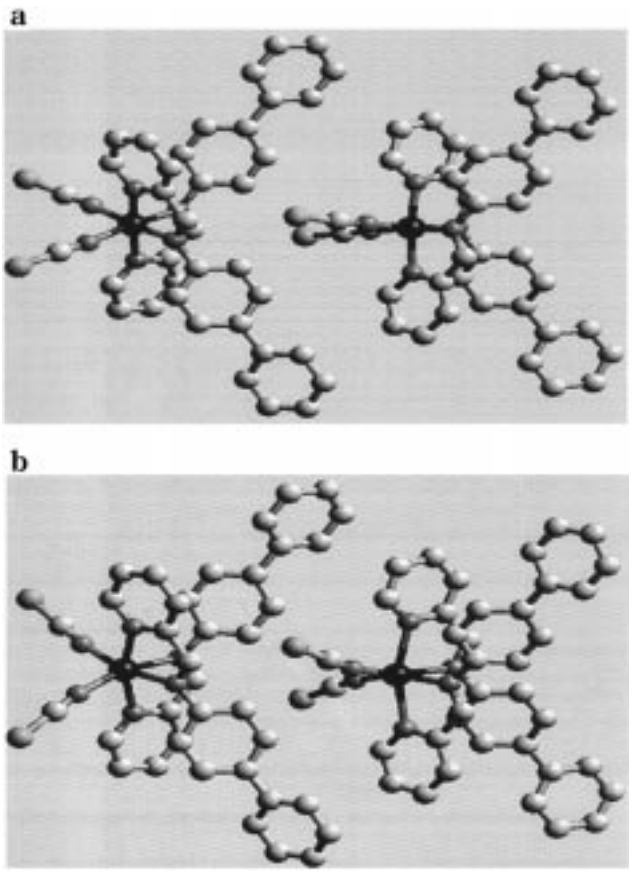

Figure 6. Intrasheet interactions for $Fe(PM\text{-}BiA)_2(NCS)_2$ at (a) 140 K and (b) 298 K.

octahedron. This is also illustrated by the N−Fe−N angles: N(26)−Fe−N(31) = 74.3(8)°, N(2)−Fe−N(31) = 90.2(3)°, and N(2)−Fe−N(26) = 96.0(3)° (Table 3).

The PM-BiA ligand is strongly nonplanar; the pyridylmethylene unit is nearly planar, whereas a dihedral angle C(22)−C(23)−N(26)−C(27) = 42.8(10)° exists between this pyridylmethylene unit and the first phenyl ring, and a dihedral angle C(12)−C(13)−C(20)−C(27) = 41.8(10)° exists between the two phenyl rings.

B. Low-Spin Crystal Structure. At 140 K the arrangement of the $Fe(PM\text{-}BiA)_2(NCS)_2$ units is quite similar to that obtained at 293 K. The spin transition affects principally the FeN_6 core geometry. The Fe−N(PM-BiA) bonds in the LS form are shorter by 0.266 Å (Fe−N(31)) and 0.285 Å (Fe−N(26)), and the Fe−N(CS) bonds by about 0.1 Å as compared to those in the HS form. The larger decrease observed for Fe−N(PM-BiA) as compared to Fe−N(CS) may be accounted for by the fact that *N*-(2-pyridylmethylene)aminobiphenyl acts as a much stronger π-electron acceptor than NCS^-, and the electron back-donation from filled metal orbitals of the LS state (t_{2g} in O_h symmetry) to vacant π^* ligand orbitals is more pronounced for Fe−N(PM-BiA) than for Fe−N(CS) bonds. Similarly, the fact that the change in the Fe−N(aminobiphenyl) bond length is more pronounced than that in the Fe−N(pyridine) bond length may be accounted for by the difference in π electron acceptor character between aminobiphenyl and pyridine groups.

The FeN_6 core is less distorted in the LS than in the HS state. The HS → LS transformation induces an increase (+6°) of the N(26)−Fe−N(31) angle and a decrease (−3°) of the N(2)−Fe−N(26) angle. It can be also noticed that the bending of the Fe−N−C(S) angles is less pronounced in the LS (C(3)−N(2)−Fe = 172.5(2)°) than in the HS state (C(3)−N(2)−Fe = 169.0(9)°), whereas the linearity of the NCS^- groups is insignificantly changed. A decrease in length, 1.162(3) and 1.134(10) Å, is observed for N−C(S) bonds when passing from 298 K down to 140 K.

A strong increase of the planarity is observed for the biphenyl unit between HS (dihedral angle C(12)−C(13)−C(20)−C(21) = 41.8(10)°) and LS (33.8(3)°) forms. Usually, a decrease of the biphenyl angle is an indication of an increase of the π stacking. The lowest energy conformation of isolated molecules of biphenyl corresponds to an intramolecular torsion angle of approximately 45°.[14] In the crystal a double well potential resulting from the competition between intramolecular and intermolecular forces has been proposed. This competition takes place between two effects: (i) intramolecular repulsion between *o*-hydrogen atoms on adjacent phenyl rings and (ii) intermolecular packing forces, which tend to restore the planarity in order to optimize the packing between molecules.[15] The increase of the π stacking in the LS form could be related not

(14) (a) Cailleau, H.; Baudour, J. L.; Meinnel, J.; Dworkin, A.; Moussa, F.; Zeyen, C. M. E. *Faraday Discuss. Chem. Soc*. **1980**, *69*, 7. (b) Tsuzuki, S.; Tanabe, K. *J. Phys. Chem*. **1991**, *95*, 139.

(15) Baker, K. N.; Fratini, A. V.; Resch, T.; Knachel, H. C.; Adams, W. W.; Socci, E. P.; Farmer, B. L. *Polymer* **1993**, *34*, 8, 1571.

only to the cell contraction but also to the change of intramolecular angles between the pyridylmethylene plane and the first phenyl ring (dihedral angle C(22)−C(23)−N(26)−C(27) = 42.8(10)° in HS versus 55.5(3)° in LS state).

Intermolecular distances shorter than van der Waals contacts as well as Fe−Fe distances between adjacent molecular units are reported in Table 4. A close look at the data reveals that C−C intermolecular contacts smaller than 3.5 Å are less numerous at room temperature than at 140 K. In the LS form very short distances exist between phenyl rings belonging to adjacent molecules (C(12)−C(12)$_{i'''}$) = 3.337 Å). The C−S intermolecular contacts are strongly affected by the change of orientation of the thiocyano groups associated with the spin transition. That leads to a significant increase of all the contacts between these groups and the carbon atoms of neighboring phenyl rings in the LS state.

Correlations between Magnetic and Structural Properties. One of the still controversial questions in the field of spin-crossover compounds concerns the factors governing the abrupt or gradual character of the spin conversion at a certain critical temperature. We would like to address this question, and for this we would like to compare the structure of Fe(PM-BiA)$_2$(NCS)$_2$ to the structures of Fe(phen)$_2$(NCS)$_2$ and Fe(btz)$_2$(NCS)$_2$, which exhibit rather abrupt and gradual transitions, respectively.[16] Fe(phen)$_2$(NCS)$_2$ and Fe(btz)$_2$(NCS)$_2$ are isostructural; they crystallize in the *Pbcn* space group both in the HS state and in the LS state, and each unit cell contains, as for Fe(PM-BiA)$_2$(NCS)$_2$, two right-handed and two left-handed enantiomers ($Z = 4$).

The spin transitions for Fe(PM-BiA)$_2$(NCS)$_2$ and for Fe(phen)$_2$(NCS)$_2$ and Fe(btz)$_2$(NCS)$_2$ are neither associated with a change in the crystal symmetry nor triggered by a structural order−disorder transition involving the NCS^- groups that would occupy different rotational positions in the high-temperature range. Only a pronounced rearrangement of the iron atom environment is detected. The main structural feature related to the spin transition seems to be the reorganization of the FeN_6 core toward a more regular octahedron when passing from the HS to the LS form, and conversely. The observation that FeN_6 is less distorted in the LS than in the HS state can be associated with a change in metal−ligand bond lengths and/or in N−Fe−N bond angles. According to Hendrickson et al.[17] the active vibrational coordinate in spin-crossover dynamics would be primarily the torsion mode. This idea derives from the work of Purcell[18] and Vanquickenborne,[19] who independently established a connection between enantiomerization of $3d^6$ transition metal derivatives and spin-state interconversion. Nevertheless, a close examination of the structural data obtained for Fe(PM-BiA)$_2$(NCS)$_2$ compared to those of Fe(phen)$_2$(NCS)$_2$ and Fe(btz)$_2$(NCS)$_2$ reveals similar modifications of the FeN_6 core for the three compounds, and points out that the abruptness of the spin transition is not mainly connected to these modifications.

According to Real et al.[16b] the key factors governing the cooperativity of the spin transition would be the number and the strength of the intermolecular interactions, and consequently the anisotropy of the structure. These authors reported that the intermolecular interactions at room temperature and their reinforcement at low temperature for Fe(btz)$_2$(NCS)$_2$ were essentially intersheet whereas they were intrasheet for Fe(phen)$_2$(NCS)$_2$. In the case of Fe(PM-BiA)$_2$(NCS)$_2$, intrasheet contacts noticeably vary with temperature. They are already strong in the HS state and are even reinforced in the LS state. Some intersheet contacts (<3.5 Å) exist at room temperature (C−C and C−S), but are not really affected by the spin transition. These data seem to indicate that the key feature of an abrupt spin transition lies in the presence of strong intrasheet contacts, which confers a two-dimensional character to the structure. A comparison between Fe(PM-BiA)$_2$(NCS)$_2$ and Fe(Phen)$_2$(NCS)$_2$ reveals a larger number of intrasheet contacts shorter than 3.5 Å in the former compound, in perfect agreement with the observation of a more abrupt spin transition.

Comparison between X-ray Powder Patterns of Samples 1 and 2. Powder diffraction was used to obtain further information on the powder samples **1** and **2**. An examination of the samples under a binocular lens indicated that sample **1** contained thin dark green grains, while sample **2** contained turquoise green ones. The diffraction pattern for **1** revealed 15 narrow peaks with a stable and narrow background, and the indexation may be considered as being reliable. The cell parameters were found to correspond to those of the single crystals in the HS state.

The diffraction pattern for **2** was less clear, with a higher background. It turns out that the indexation might be questionable. However, it is clear that this phase **2** is not the same as phase **1**, as no common peak between the two phases could be found. The best cell was obtained from the 12 more intense peaks; it corresponds to a monoclinic phase with $a = 14.37(2)$ Å, $b = 19.85(2)$ Å, $c = 7.91(2)$ Å, $\beta = 94.1(1)°$, $V = 2252$ Å^3.

Thermogravimetric Analysis and DSC Measurements. A thermogravimetric analysis was performed on the powder sample **1** in the 298−573 K temperature range. This analysis indicates an insignificant loss of mass until 473 K (0.45%) and therefore confirms the absence of solvent molecules in the lattice. Above 473 K the compound begins to decompose.

The heat capacity measurements were carried out in the 193−153 K temperature range. The temperature dependences of the molar heat capacity, C_p, in the cooling and warming modes are shown in Figure 7. $T_{1/2}\downarrow$ and $T_{1/2}\uparrow$ were determined as the temperatures for which $\partial C_p/\partial T$ is maximum and found as $T_{1/2}\downarrow = 173.10$ K and $T_{1/2}\uparrow = 175.80$ K. The temperature uncertainty is estimated as ±0.25 K. It turns out that these DSC curves confirm the presence of a weak thermal hysteresis. Its width, however, is only 3 K in the DSC experiments, as compared to 5 K in the magnetic measurements.

The enthalpy and entropy variations, ΔH and ΔS, respectively, associated with the spin transition were determined from the DSC curves. Their values are given in Table 5, together with the values found for Fe(phen)$_2$(NCS)$_2$ by Sorai and Seki from abiabatic calorimetry[20a] and by Zarembowitch and co-workers from DSC.[20b] ΔS is significantly larger for our compound than for the two phen derivatives. The electronic contribution, $\Delta S_{el} = R \ln(\Omega_{HS}/\Omega_{LS}) = 13.38$ J K^{-1} mol^{-1} (Ω_{HS} and Ω_{LS} being the spin degeneracies of the HS and LS states, respectively), is identical for the three compounds. Furthermore, the modifications of the FeN_6 core (bond lengths and angles) between HS and LS states are very similar for the three compounds, so that the $\Delta S_{vib,intra}$ contributions arising from intramolecular vibrations may be assumed to be close to each other. If it is so, the differences of ΔS would be essentially due to the differences of $\Delta S_{vib,inter}$ contributions arising from phonons. Such an

(16) (a) Gallois, B.; Real, J.-A.; Hauw, C.; Zarembowitch, J. *Inorg. Chem.* **1990**, *29*, 1152. (b) Real, J.-A.; Gallois, B.; Granier, T.; Suez-Panamá, F.; Zarembowitch, J. *Inorg. Chem.* **1992**, *31*, 4972.
(17) McCusker, J. K.; Rheingold, A. L.; Hendrickson, D. N. *Inorg. Chem.* **1996**, *35*, 2100.
(18) Purcell, K. F. *J. Am. Chem. Soc.* **1996**, *101*, 5147.
(19) Vanquickenborne, L. G.; Pierloot, K. *Inorg. Chem.* **1981**, *20*, 3673.
(20) (a) Sorai, M.; Seki, S. *J. Phys. Chem. Solids* **1974**, *35*, 555. (b) Martin, J. P.; Dworkin, A.; Zarembowitch, J. Private communication.

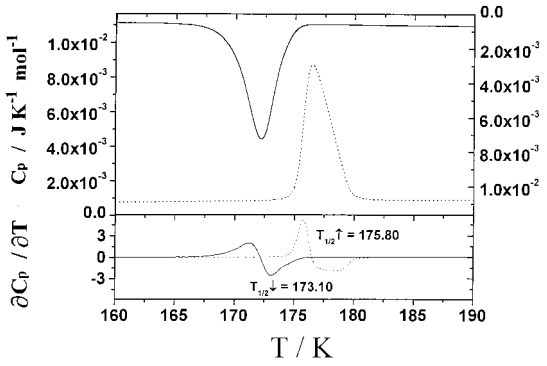

Figure 7. C_p and $\partial C_p/\partial T$ versus T curves for the powder sample **1**.

Table 5. Thermodynamic Quantities Associated with the Spin Transition in Three Bis(thiocyanato) Iron(II) Compounds

	T_c (K)	ΔH (kJ mol^{-1})	ΔS (J K^{-1} mol^{-1})
Fe(PM-BiA)$_2$(NCS)$_2$	$T_{1/2}\downarrow = 168^c$	10.06	59.88
	$T_{1/2}\uparrow = 173^c$	10.05	58.09
Fe(phen)$_2$(NCS)$_2$[a]	176.29	8.60	48.78
Fe(phen)$_2$(NCS)$_2$[b]	176	7.90	45.4

[a] Adiabatic calorimetry.[20a] [b] From ref 20b. [c] From magnetic measurements.

analysis is in line with the fact that there are more intrasheet contacts in Fe(PM-BiA)$_2$(NCS)$_2$ than in the phen derivatives, which confers a more pronounced two-dimensional character to this compound.

UV−Visible Spectroscopy. The UV−visible electronic absorption spectra for Fe(PM-BiA)$_2$(NCS)$_2$ were recorded at room temperature under various experimental conditions, namely, in a KBr pellet, in a cellulose acetate film, and in solution in acetonitrile and butyronitrile. The spectra show three bands; in acetonitrile these are situated at 256 nm ($\epsilon = 38\,000$ L mol^{-1} cm^{-1}), 337 nm ($\epsilon = 22\,600$ L mol^{-1} cm^{-1}), and 585 ($\epsilon = 1230$ L mol^{-1} cm^{-1}). The band at 585 nm can be attributed to a low-spin metal-to-ligand charge-transfer band (^{1}MLCT). The shorter Fe−N bond lengths in the LS state lead to much larger overlaps between metal and ligand centered orbitals than in the HS state. Consequently, the bands associated with the HS state are generally weak and masked by those associated with the LS state. The two bands at higher energy are $\pi-\pi^*$ transitions of the organic ligand.

Figure 8 presents the temperature dependence of the UV−visible spectra of Fe(PM-BiA)$_2$(NCS)$_2$ both in butyronitrile and embedded in cellulose acetate. The HS → LS transition results in a strong enhancement of the ^{1}MLCT band around 640 nm. The color of the compound remains unchanged, in contrast with what happens for the tetrazole and triazole iron(II) derivatives. In these latter species, the spin transition is accompanied by a change of color, between violet (or pink) in the LS state and white in the HS state.[3,4,6] The presence of aromatic rings conjugated with the iron ion results in a strong ^{1}MLCT band, which prevents the thermochromism of the system.

Photomagnetic Properties. A. LIESST Effect. The LIESST experiments were carried out on the powder sample **1**. The results are shown in Figure 9. The sample was first slowly cooled from ca. 100 K down to 10 K, and the $\chi_M T$ versus T curve was recorded. This curve confirms that the compound is in the LS state. The sample was then irradiated at 10 K with a red light ($\lambda = 647.1-676.4$ nm) for 1 h with an intensity of 50 mW; $\chi_M T$ was found to increase rapidly, then to reach a value of ca. 0.7 cm^3 K mol^{-1}, indicating a partial conversion

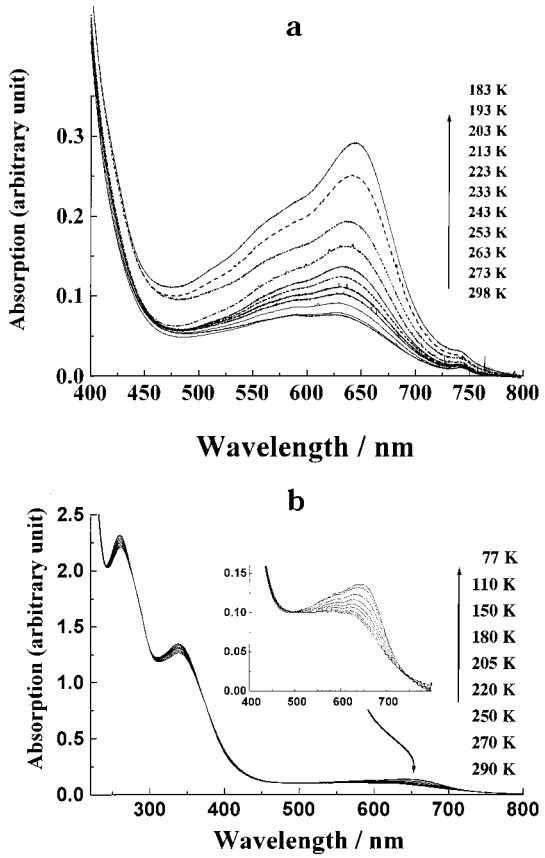

Figure 8. Temperature dependence of the UV−visible electronic absorption spectra for Fe(PM-BiA)$_2$(NCS)$_2$ (a) in butyronitrile; (b) embedded in cellulose acetate.

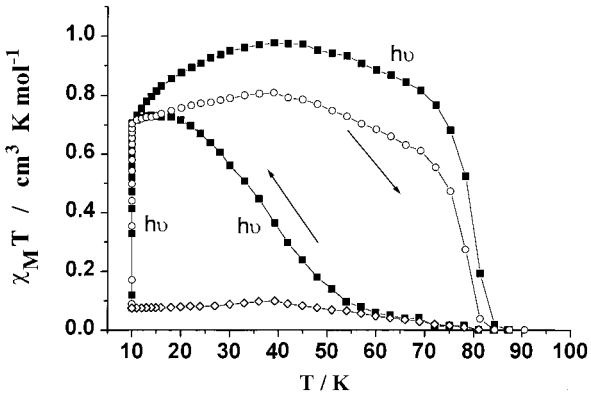

Figure 9. $\chi_M T$ versus T and light irradiation for the powder sample **1** (0.35 mg): (◇) data in the cooling mode without irradiation; (○) data obtained with irradiation for 1 h at 10 K and then without irradiation in the warming mode; (■) data obtained with irradiation for 1 h at 10 K and then with irradiation in both the warming and cooling modes.

(≈20%) of the LS state into the HS state, according to the well-known LIESST process.[21]

The population of this metastable HS state can be also observed at 10 K by using other wavelength excitations: i.e., $\lambda = 488.0-514.5$ nm, $\lambda = 530.9$ nm, or even $\lambda = 752.5-799.3$ nm. Such a LIESST effect in the 752.5−799.3 nm range differs from what was observed for the tetrazole iron(II) derivatives. As a matter of fact, these latter compounds exhibit rather the

(21) (a) Decurtins, S.; Gütlich, P.; Köhler, C. P.; Spiering, H.; Hauser, A *Chem. Phys. Lett.* **1984**, *105*, 1. (b) Decurtins, S.; Gütlich, P.; Hasselbach, K. M.; Hauser, A.; Spiering, H. *Inorg. Chem.* **1985**, *24*, 2174.

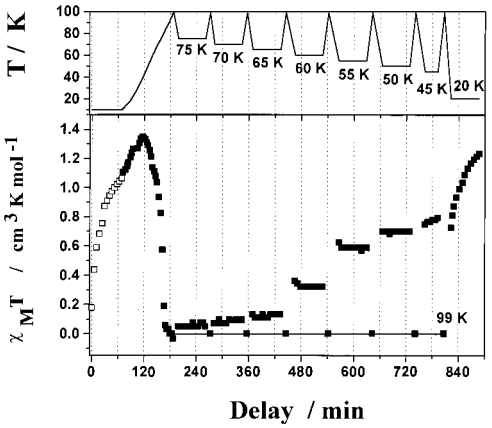

Figure 10. Magnetic properties of the powder sample **1** (0.21 mg) versus temperature and light irradiation.

reverse-LIESST effect.[22] The most straightforward explanation for this difference is that the weak $^5T_2 \rightarrow {}^5E$ absorption band is totally overlapped by the intense ^{1}MLCT band (see Figure 8). The aromatic rings of the organic ligand play the role of antenna, allowing observation of the LIESST effect in a large wavelength range via the ^{1}MLCT band.

B. Light-Induced Thermal Hysteresis (LITH). We have seen that, after 1 h of irradiation at 10 K with a red light (λ = 647.1−676.4 nm, 50 mW), 20% of HS molecules were formed. Without further irradiation (mode OFF), the temperature was slowly increased, and the temperature dependence of $\chi_M T$ was recorded. $\chi_M T$ remains nearly constant as T increases from 10 K up to 70 K. The $\chi_M T$ value at 70 K is 0.61 cm^3 K mol^{-1}, corresponding to about 17% of HS molecules, then drops rapidly as the temperature is increased further, and eventually reaches a value close to 0 around 80 K. The critical LIESST temperature may then be defined as T_{liesst} = 80 K.

Let us now examine what happens as the light irradiation is maintained (mode ON) during warming and then cooling of the sample. The temperature dependence of $\chi_M T$ in mode ON is rather similar to that in mode OFF when the temperature is increased from 10 to 100 K. The slightly larger $\chi_M T$ values in mode ON are probably due to the longer time of irradiation. Let us notice here that the irradiation may locally heat the sample, whose temperature would be higher than that indicated by the thermometer. This effect would tend to decrease the $\chi_M T$ signal, in contrast to what is observed. The temperature dependence of $\chi_M T$ when the sample is being cooled in mode ON reveals a new type of hysteresis. The HS molar fraction is close to 0 as T is lowered down to 60 K, then progessively increases as T is lowered further down to 10 K, and eventually reaches 20%. It follows that the two curves in mode ON in the warming and cooling regime, respectively, are not identical, as shown in Figure 9. Measurements in mode ON were also performed as a function of time. The results are depicted in Figure 10. After irradiation at 10 K during 1 h, the temperature was increased up to 99 K, where $\chi_M T$ is 0. Then, during nearly 1 h the temperature was fixed at 75, 70, 65, 60, 55, 50, 45, and 20 K, successively. Between two successive temperatures the sample was warmed to 99 K, and maintained for 5 min at that temperature in order to erase the information, i.e., to come back to $\chi_M T$ = 0. Let us explain this behavior; at 50 K, the $\chi_M T$ value in the warming regime is 1.28 cm^3 K mol^{-1}, while even after 1 h of light irradiation at that temperature, the $\chi_M T$ value in the cooling regime does not overcome 0.70 cm^3 K mol^{-1}.

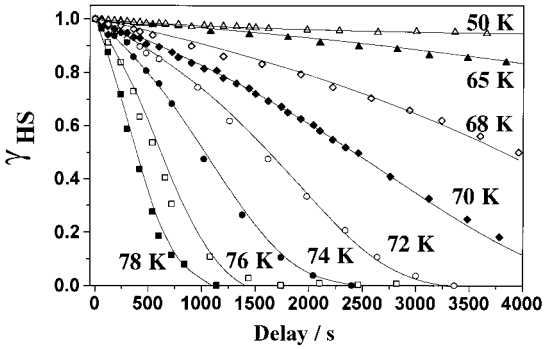

Figure 11. Time dependence at various temperatures of the HS molar fraction, γ_{HS}, generated by light irradiation at 10 K. Each point represents the HS molar fraction deduced from the $\chi_M T$ value measured with the SQUID magnetometer during around 30 s. The HS → LS relaxation curves are fitted with eqs 2−4 for T ≥ 65 K and eq 5 for 5 K < T < 65 K.

Such results clearly demonstrate the existence of a photoinduced bistability for Fe(PM-BiA)$_2$(NCS)$_2$. We propose to call this phenomenom light-induced thermal hysteresis (in short, LITH).

Recently, Gütlich and Hauser reported that for [Fe(etz)$_6$](BF$_4$)$_2$, etz = 1-ethyltetrazole, a hysteresis subsequent to light irradiation at 820 nm existed, with 72 < $T_{1/2}$ < 80 K.[23] These authors explained such a situation by the presence of two sites, which relaxed differently. In our case, the LITH effect is more pronounced, with 35 < $T_{1/2}$ < 77 K. A very simple explanation may be suggested. In mode ON two effects are operative, the light-induced trapping of the system in the metastable HS state, on the one hand, and the relaxation from this HS state toward the ground LS state, on the other hand. When $T > T_{liesst}$, the HS → LS relaxation is so fast that light-induced trapping in the metastable HS state cannot be observed with our setup. At a given temperature between the lowest temperature (10 K) and T_{liesst}, the amount of HS molecules will depend on the amount of HS molecules at the initial stage. Let us explain this naive idea in the simple case where at a given temperature T_0 one molecule is trapped in the HS state when one molecule is relaxed toward the LS state. In the warming mode the HS molar fraction, γ_{HS}, may be assumed to be normalized to unity at 10 K, and this value will remain close to unity at T_0. In fact, an increase of γ_{HS} will be expected due to the larger time of irradiation from 10 K to T_0, where the trapping process is more active than the relaxation pathway. In the cooling mode the γ_{HS} value at T_{liesst} is 0, and this value will remain 0 at T_0. A light-induced thermal hysteresis is then observed.

C. HS → LS Relaxation. The dynamics of the LIESST effect for Fe(PM-BiA)$_2$(NCS)$_2$ is rather slow in the 5−78 K temperature range, and the time dependence of $\chi_M T$ can be studied with the SQUID setup. The decays of the HS molar fraction, γ_{HS}, versus time at various temperatures are represented in Figure 11; γ_{HS} is deduced from the $\chi_M T$ value through eq 1, and it is normalized to unity at time 0. An analysis of these data indicates that the relaxation curves can be satisfactorily fitted with an Arrhenius law up to 60 K, while deviations from single-exponential behavior were observed at higher temperatures (60 < T < 80 K); the time dependence of the HS molar fraction then follows a sigmoidal-type behavior.

It is well established that the HS → LS relaxation for spin-transition compounds in the solid state is strongly influenced by cooperative effects.[23] Hauser demonstrated by optical

(22) Hauser, A. *Chem. Phys. Lett.* **1986**, *124*, 543.

(23) Hinek, R.; Spiering, H.; Gütlich, P.; Hauser, A. *Chem. Eur. J.* **1996**, *2*, 1435.

spectroscopy that in the highly diluted single crystal $[Fe_xZn_{1-x}(ptz)_6](BF_4)_2$ ($x = 0.1$) the γ_{HS} versus T curves followed first-order kinetics, whereas for pure $[Fe(ptz)_6](BF_4)_2$ compound sigmoidal relaxation curves were found.[1f] Such curves can be interpreted as a self-acceleration of the HS → LS relaxation as γ_{HS} decreases. Each HS ion in a crystal acts as internal pressure ("lattice pressure") and increases the relaxation rate. This "lattice pressure" is caused by the large reduction in size of the spin-crossover compound as it converts from HS to LS.[24,25] The rate of disappearance of the HS form is given by eqs 2−4.

$$-\frac{d\gamma_{HS}}{dt} = k_{HL}(\gamma_{HS},T)\gamma_{HS} \quad (2)$$

$$k_{HL}(\gamma_{HS},T) = k_{HL}(T)\exp\left(-\frac{E_a^*}{k_BT}\gamma_{HS}\right) \quad (3)$$

$$k_{HL}(T) = k_{HL}{}^0\exp\left(-\frac{E_a}{k_BT}\right) \quad (4)$$

In eq 2, $k_{HL}(\gamma_{HS},T)$ is the rate constant for the HS → LS conversion. This parameter is a function of γ_{HS} and T. E_a* stands for the additional activation energy due to cooperativity, and $k_{HL}(T)$ for the relaxation rate at T (eq 3). Finally, E_a is the activation energy associated with the HS → LS relaxation, and $k_{HL}{}^0$ the preexponential factor (eq 4).

If the relaxation of a molecule from the metastable HS state to the LS state after LIESST is very slow, then the modification of the internal pressure can be neglected, and eq 2 is valid; the rate constant $k_{HL}(T)$ is a mere function of T (see eq 5). The activation energy, E_a, and the preexponential factor, $k_{HL}{}^0$, are obtained from eq 4.

$$\gamma_{HS}(t) = \exp(-k_{HL}(T)t) \quad (5)$$

In the 5−60 K temperature range, the HS → LS relaxation is very slow. However, it can be measured with our photomagnetic equipment; for instance, at 10 K γ_{HS} varies about 2% within 9 h, and the corresponding change of χ_MT is 1 order of magnitude larger than the background of the instrument. The HS → LS relaxation curves for $Fe(PM\text{-}BiA)_2(NCS)_2$ can be reasonably well fitted by a single exponential (eq 5). The $k_{HL}(T)$ values obtained from a least-squares fitting of the experimental data are listed in Table 6. At $T > 60$ K, the HS → LS relaxation kinetics for $Fe(PM\text{-}BiA)_2(NCS)_2$ after laser excitation is fast, and eqs 2 and 3 were utilized to analyze the sigmoidal-type behavior. Least-squares fitting of the experimental data with these equations leads to the $k_{HL}(T)$ and E_a* values of Table 6. The mean additional activation energy E_a* is found as about 118 cm^{-1}. Such a value can be compared to the mean value of 60 cm^{-1} reported for $[Fe(bptn)_2(NCS)_2]$ (bptn = 1,7-bis(2-pyridyl)-2,6-diazaheptane)[26] and of 164 cm^{-1} for $[Fe(ptz)_6](BF_4)_2$.[27]

Figure 12 presents the $\ln[k_{HL}(T)]$ versus $1/T$ plot. A thermally activated relaxation behavior at elevated temperatures and a nearly temperature independent relaxation behavior at low temperatures can be observed. For $T \geq 55$ K, the $\ln[k_{HL}(T)]$ versus $1/T$ plot gives a straight line, with $k_{HL}{}^0 = 8.7 \times 10^5$ s^{-1} and $E_a = 980 \pm 10$ cm^{-1}. Hauser et al.[27] observed a linear dependence for $[Fe(ptz)_6](BF_4)_2$ ($E_a = 797$ cm^{-1} and $k_{HL}{}^0 = 10^5$ s^{-1}), whereas a pronounced deviation from linearity was reported for $[Fe(bpp)_2(NCS)_2]$ (bpp = 2,6-bis(pyrazol-3-yl)-pyridine), due to a crystallographic phase transition.[28] For 5 K $< T <$ 55 K, the $\ln[k_{HL}(T)]$ versus $1/T$ plot gives a straight line with a 0 slope and a preexponential factor $k_{HL}{}^0$ of 4.6×10^{-6} s^{-1}. The rate constant for the HS → LS relaxation as T approaches the absolute 0 is an important diagnostic for Fe^{II} spin-crossover compounds. In the case of $Fe(PM\text{-}BiA)_2(NCS)_2$ the $k_{HL}{}^0$ value is found to be unreasonably small, which suggests that tunneling is the predominant mechanism for the relaxation below 65 K.

In the theory of nonadiabatic multiphonon relaxation[29] the low-temperature tunneling rate depends on both the Huang−Rhys factor, S (see eqs 6 and 7), which is a measure of the horizontal displacement of the potentials of the HS and LS states, and the energy gap between the lowest vibronic levels of the HS and LS states, assumed to vary as $T_{1/2}$. Recently, Hauser et al.[30] observed for a series of FeN_6 spin-crossover compounds

Table 6. Rate Constants $k_{HL}(T)$ (s^{-1}) and Additionnal Activation Energies E_a* (cm^{-1}) as a Function of Temperature for $Fe(PM\text{-}BiA)_2(NCS)_2$

T	$k_{HL}(T)$	E_a*
5[a]	5×10^{-6}	
10[a]	4.9×10^{-6}	
15[a]	4.4×10^{-6}	
20[a]	3.3×10^{-6}	
30[a]	3.5×10^{-6}	
40[a]	3.8×10^{-6}	
50[a]	1×10^{-5}	
55[a]	5.2×10^{-5}	
60[a]	4×10^{-5}	
65[b]	4.5×10^{-4}	110
68[b]	8.6×10^{-4}	101
70[b]	1.2×10^{-3}	93
72[b]	3.6×10^{-3}	143
74[b]	4.5×10^{-3}	133
75[b]	6.0×10^{-3}	118
76[b]	6.3×10^{-3}	116
78[b]	9.7×10^{-3}	126
80[c]		

[a] HS → LS relaxation curves are fitted according to eq 5, because of the exponential behavior. [b] Sigmoidal relaxation curves fitted with eqs 2−4. [c] At higher temperature HS → LS kinetics is too fast to be observed.

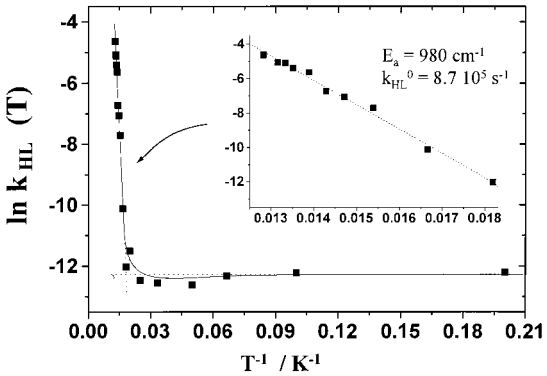

Figure 12. $\ln k_{HT}(T)$ versus $1/T$ curve. For $T \geq 55$ K, a straight line is obtained with $k_{HL}{}^0 = 8.7 \times 10^5$ s^{-1} and $E_a = 980 \pm 10$ cm^{-1}. For 5 K $< T <$ 55 K, the $\ln[k_{HL}(T)]$ versus $1/T$ plot gives a straight line with a 0 slope and a preexponential factor $k_{HL}{}^0$ of 4.6×10^{-6} s^{-1} ($\ln k_{HL}{}^0 = -12.3$).

(24) Hauser, A. *Chem. Phys. Lett*. **1992**, *192*, 65.
(25) Hinek, R.; Gütlich, P.; Hauser, A. *Inorg. Chem.* **1994**, *33*, 567.
(26) Buchen, T.; Toflund, H.; Gütlich, P. *Chem. Eur. J.* **1996**, *2*, 1129.
(27) Hauser, A.; Gütlich, P.; Spiering, H. *Inorg. Chem.* **1986**, *25*, 4245.
(28) Buchen, T.; Gütlich, P.; Goodwin, H. A. *Inorg. Chem*. **1994**, *33*, 4573.
(29) Buhks, E.; Navon, G.; Bixon, M.; Jortner, J. *J. Am. Chem. Soc*. **1980**, *102*, 2918.
(30) Hauser, A. *Coord. Chem. Rev.* **1991**, *111*, 275.

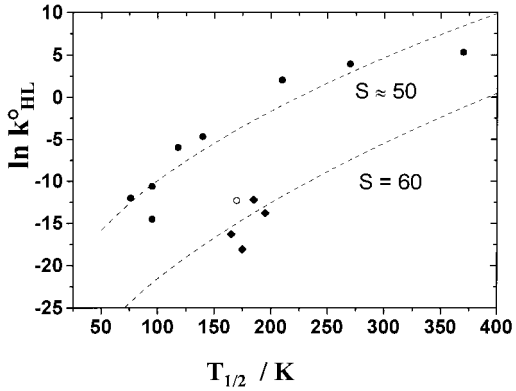

Figure 13. Variation of ln k_{HT}^0 versus $T_{1/2}$ for spin-crossover compounds with FeN_6 (●) and $Fe^{II}P_4X_2$ (◆) cores, and for Fe(PM-BiA)$_2$(NCS)$_2$ (○). The dashed lines are the results calculated for FeN_6 compounds with $S \approx 50$ and for the $Fe^{II}P_4X_2$ and Fe(PM-BiA)$_2$(NCS)$_2$ compounds with $S = 60$, assuming a linear relationship between $\Delta E°_{HL}$ and $T_{1/2}$ (see text).

that k_{HL}^0 and $T_{1/2}$ were correlated; more precisely, k_{HL}^0 increases as $T_{1/2}$ increases. This behavior was defined as the inverse energy-gap law. For Fe(PM-BiA)$_2$(NCS)$_2$, $T_{1/2}$ is around 175 K, and therefore a fast relaxation would be expected to occur at low temperatures. In fact, the relaxation is very slow (T_{liesst} = 80 K), and at low temperatures the calculated k_{HL}^0 ($= 4.6 \times 10^{-6}$ s^{-1}) does not obbey the inverse energy-gap law[30] (see Figure 13). The tunneling rate constant for the HS → LS relaxation at low-temperatures is given by

$$k_{HL}^{\ 0} = \frac{2\pi}{\hbar^2\omega}(\beta_{HL})^2\Omega_{LS}\left(\frac{s^p e^{-S}}{p!}\right) \qquad (6)$$

$$S = \frac{1}{2} f \frac{\Delta Q^2}{\hbar\omega} \quad \text{with} \quad \Delta Q = \sqrt{6}\Delta r_{HL} \qquad (7)$$

where β_{HL} is the electronic tunneling matrix element, $\hbar\omega$ is the frequency of the breathing vibration of the FeN_6 core, $p = \Delta E°_{HL}/\hbar\omega$ is the reduced energy gap, and S is the Huang−Rhys factor. Assuming a linear dependence between $\Delta E°_{HL}$ and $T_{1/2}$ and using eq 6 results in $S \approx 50$, $\beta_{HL} = 150$ cm^{-1}, and $\hbar\omega = 250$ cm^{-1}.

Figure 13 also shows the ln k_{HL}^0 versus $T_{1/2}$ plot for compounds with the $Fe^{II}P_4X_2$ core[31] together with Fe(PM-BiA)$_2$(NCS)$_2$. $S \approx 60$ fits the data reasonably well. The low-temperature tunneling for Fe(PM-BiA)$_2$(NCS)$_2$ is much slower than for the other FeN_6 compounds, because of a larger Huang−Rhys factor. This situation is probably due to to a more pronounced change of Fe−N(organic ligand) bond lengths for our compounds (0.28 Å) than for the other FeN_6 compounds (0.16−0.21 Å). The same observation has been made concerning the compounds with the $Fe^{II}P_4X_2$ core, whose Fe−P bond length varies by 0.27 Å between LS and HS states.[31] Along the same line, the fact that the lifetime of the metastable HS state is longer for Fe(PM-BiA)$_2$(NCS)$_2$ may be attributed to the larger horizontal displacement between the LS and HS potential energy wells, as compared to the other FeN_6 species.

Concluding Remarks

Fe(PM-BiA)$_2$(NCS)$_2$ exhibits an exceptionally abrupt thermally induced spin transition. Both in the cooling and in the warming modes more than 90% of the molecules undergo a transition between LS and HS states within ca. 1.5 K. The thermal hysteresis width, however, is limited to 5 K, with $T_{1/2}{\downarrow}$ = 168 K and $T_{1/2}{\uparrow}$ = 173 K. It is difficult to compare the abruptnesses of all the spin-crossover compounds reported so far. If we restrict ourselves to the family of the bis(thiocyanato) iron(II) derivatives, Fe(PM-BiA)$_2$(NCS)$_2$ clearly undergoes the most abrupt transition. Until the present, Fe(phen)$_2$(NCS)$_2$ was considered as the archetype of compounds exhibiting a discontinuous change of spin state. Hereafter, Fe(PM-BiA)$_2$(NCS)$_2$ could play this role.

The spin transition in the case of Fe(PM-BiA)$_2$(NCS)$_2$ may be considered as being intrinsic. As a matter of fact, it is not triggered by a crystallographic phase transition. The orthorhombic space group *Pccn* is retained in both spin states. What seems to be crucial to explain the strong cooperativity of the compound is the two-dimensional character of the crystal structure resulting from close contacts between aromatic rings belonging to adjacent molecules. Interestingly, the entropy variation associated with the LS → HS transformation, ΔS = 58 J K^{-1} mol^{-1}, is the highest found for bis(thiocyanato) iron(II) derivatives. Most likely, the short intrasheet contacts result in a strong $\Delta S_{vib,inter}$ contribution due to phonons.

For the first time in our research group, we also explored the photomagnetic properties, using a setup in which the SQUID cavity is coupled to a multimode laser through an optical fiber. The now well documented LIESST effect was obtained at 10 K, with a critical LIESST temperature, T_{liesst}, of ca. 80 K. A slow rate of quantum mechanical tunneling from the metastable HS state to the stable LS state was observed. This behavior was correlated with the unusually large change in Fe−N(organic ligand) bond lengths associated with the spin transition. In addition, a new phenomenon was observed, namely, a light-induced thermal hysteresis (LITH). Under irradiation below T_{liesst} the temperature dependence of the HS molar fraction is not the same in the cooling and warming modes. A very simple, rather naive explanation has been suggested. Of course, this LITH effect requires more studies, and we intend to return to this phenomenon in a subsequent paper.

Supporting Information Available: Tables giving crystallographic data, positional parameters, and U values (3 pages). Ordering information is given on any current masthead.

IC980107B

(31) Wu, C.-C.; Jung, J.; Gantzel, P. K.; Gütlich, P.; Hendrickson, D. N. *Inorg. Chem.* **1997**, *36*, 5339.